



Article

Carbon Quantum Dots Modified (002) Oriented $\text{Bi}_2\text{O}_2\text{CO}_3$ Composites with Enhanced Photocatalytic Removal of Toluene in Air

Junping Ding ^{1,2}, Huanchun Wang ^{3,*} , Yidong Luo ¹, Yushuai Xu ¹, Jinsheng Liu ², Ruichu Lin ², Yuchen Gao ² and Yuanhua Lin ^{1,*}

¹ State Key Laboratory of New Ceramics and Fine Processing, School of Materials Science and Engineering, Tsinghua University, Beijing 100084, China; djp15@mails.tsinghua.edu.cn (J.D.); ydluozd@163.com (Y.L.); xuyushuai5736@163.com (Y.X.)

² China Astronaut Research and Training Center, Beijing 100094, China; goldsix@sohu.com (J.L.); linruichu@163.com (R.L.); accgao@163.com (Y.G.)

³ High-Tech Institute of Xi'an, Xi'an 710025, China

* Correspondence: wang-hc12@tsinghua.org.cn (H.W.); linyh@mail.tsinghua.edu.cn (Y.L.); Tel.: +86-10-6277-3741 (Y.L.)

Received: 9 August 2020; Accepted: 4 September 2020; Published: 9 September 2020



Abstract: In work, (002) oriented flower-like $\text{Bi}_2\text{O}_2\text{CO}_3$ (BOC) composites are synthesized by a facile chemical route and carbon quantum dots (CQDs) are modified on their surfaces through a hydrothermal method. The synthesized samples (CQD/BOC) are characterized by X-ray diffraction (XRD), SEM, X-ray photoelectron spectroscopy (XPS), UV-Vis diffuser reflectances (DRS), BET and TEM/HRTEM. The morphologies of CQD/BOC composites are the flower-like shapes, the irregular flaky structures and the fine spherical particles of CQDs attached. Photocatalytic performances were investigated in terms of removing gaseous toluene at a concentration of 94.3ppm in air, with the assistance of CQD/BOC under artificial irradiation. Our results show that CQDs modified (002) oriented $\text{Bi}_2\text{O}_2\text{CO}_3$ exhibits good photocatalytic activity for toluene decomposition, which can be attributed to the enhanced efficient charge separation. A certain ratio composite photocatalyst (BOC-CQD-15) shows a toluene removal rate of 96.62% in three hours, as well as great stability. CO_2 was verified to be the primary product. The oriented flower-like $\text{Bi}_2\text{O}_2\text{CO}_3$ with carbon quantum dots on the surface shows great potential in the field of solar driven air purification.

Keywords: $\text{Bi}_2\text{O}_2\text{CO}_3$; carbon quantum dots (CQDs); crystal orientation; toluene removal; photocatalysis

1. Introduction

Volatile organic compounds (VOCs) are one of the major gas pollutants in indoor air, including various alcohols, aromatics (benzene, ethylbenzene, toluene, xylene, etc.), aldehydes (acetaldehyde, formaldehyde, etc.) and halocarbons, which put humans health at great risks [1–3]. Many technologies are used to remove gas pollutants, such as adsorption by carbon-based filter media, ionization, ultraviolet degradation, plasma technology, catalytic degradation and the photocatalysis method [4–6]. Among all these technologies, photocatalysis may be a promising technique for indoor air purification, because harmless CO_2 and H_2O are the main products of pollutant degradation [7].

Bi-based photocatalysts have drawn increasing attention recently, because of their good chemical stability under visible light irradiation and unique electronic band structure. The hybridization of O 2p and Bi 6s orbitals in Bi-based photocatalysts composites results in a well-dispersed valence band (VB). In the meantime, the lone-pair distortion of Bi 6s orbitals can cause the pronounced overlap of O 2p and Bi 6s orbitals, which would increase the mobility of charge carriers and decrease the band

gap [8–10]. Considering the stability of Bi^{3+} , most studies of Bi-based photocatalysts have focused on Bi^{3+} -containing compounds, such as Bi_2O_3 , BiVO_4 , Bi_2WO_6 , BiOX ($X = \text{Cl}, \text{Br}, \text{I}$), $\text{Bi}_2\text{O}_2\text{CO}_3$ (BOC) and so on [11–15].

As a member of Bi-based photocatalysts, $\text{Bi}_2\text{O}_2\text{CO}_3$ has been used for health care and in medical fields due to its no toxicity merit for a long time [16]. For first time, $\text{Bi}_2\text{O}_2\text{CO}_3$ was found that could display good photocatalytic activity under UV light irradiation for the degradation of methyl orange aqueous solution in 2010 [17]. $\text{Bi}_2\text{O}_2\text{CO}_3$ crystallizes in a body-centered orthorhombic Imm2 space group with lattice parameters of $a = 3.865 \text{ \AA}$, $b = 3.862 \text{ \AA}$ and $c = 13.675 \text{ \AA}$ [18]. $\text{Bi}_2\text{O}_2\text{CO}_3$ has a featured layer structure, in which the CO_3^{2-} layers are alternately intercalated between $[\text{Bi}_2\text{O}_2]^{2+}$ polycation layers. The separate $[\text{Bi}_2\text{O}_2]^{2+}$ and CO_3^{2-} layers favor an internal electric field (IEF), which can greatly improve the charge separation rate [19]. Due to its particular layer structure, suitable band gap, excellent photocatalytic activity and long-term stability, $\text{Bi}_2\text{O}_2\text{CO}_3$ has drawn considerable attention for its promising application in the photocatalysis field [20]. However, $\text{Bi}_2\text{O}_2\text{CO}_3$ has a wide band gap (2.8–3.5) eV [21] and it can only response ultraviolet light of the solar light, which greatly restricts its practical application under full solar light. To solve this problem, several strategies have been investigated, mainly focusing on doping elements [22–24], Crystal facet engineering [18,25,26] and Constructing heterostructures [27–29]. As an up-conversion material, Carbon quantum dots (CQDs) can absorb NIR light at specific wavelengths and emit UV or visible light, which provide an indirect route for the use of NIR light in the photocatalytic process. Therefore, full-light-response photocatalytic heterostructures composed of CQDs and semiconductors, including CQDs/ TiO_2 , CQDs/ Cu_2O , CQDs/ Fe_2O_3 and CQDs/ Ag_3PO_4 , have recently been developed [30–33]. Thus, we were inspired that CQDs would extend the photo response range of $\text{Bi}_2\text{O}_2\text{CO}_3$ through establishing a heterostructure.

Herein, we report a facile chemical method to fabricate $\text{Bi}_2\text{O}_2\text{CO}_3$ composites with (002) facet exposed and a hydrothermal route to modified carbon quantum dots on the surface of $\text{Bi}_2\text{O}_2\text{CO}_3$. The morphologies of synthesized composites (CQD/BOC) were flower-like shapes, irregular flaky structures and fine spherical particles. Their photocatalytic properties for removal toluene in air under the artificial irradiation are investigated comparatively. Based on the close correlation between the structure characteristics and physicochemical properties of the material, BOC-CQD-15 has proved to be most active, with a removal rate of up to 96.62%. Permineralization of toluene in photocatalysis is proposed based on the characterization; CO_2 was verified to be the primary product. This work may probably extend to the application of oriented flower-like $\text{Bi}_2\text{O}_2\text{CO}_3$ with carbon quantum dots on the surface in air purification.

2. Materials and Methods

2.1. Fabrication of CQD/BOC Membranes

All the chemical reagents in this work were analytical-grade and used without any further purification.

2.1.1. Preparation of $\text{Bi}_2\text{O}_2\text{CO}_3$ Composites

An amount of Bi_2O_3 (99.99%, Aladdin Industrial Corporation, Shanghai, China) was dissolved in 1mol/L HNO_3 (GR, Sinopharm Chemical Reagent Co., Ltd., Shanghai, China) solution through the ultrasonic sound. The solution was put in a 20 °C water bath until the equalization of temperature. Then, 0.6mol/L Na_2CO_3 (RA, Sinopharm Chemical Reagent Co., Ltd., Shanghai, China) solution was added to the above solution at a speed of 30mL/min, so as to obtain a pH = 7 uniform solution, while stirring manually. Finally, the product was centrifuged, washed with deionized water and ethyl alcohol and dried at 70 °C in an oven to obtain $\text{Bi}_2\text{O}_2\text{CO}_3$ composites labeled as BOC.

2.1.2. Preparation of CQDs

The CQDs were obtained through a hydrothermal route [34]. Glucose (1 g, AR, Sinopharm Chemical Reagent Co., Ltd., Beijing, China) was dissolved into deionized water (80 mL) to obtain a homogeneous solution. Then, the solution was treated under a hydrothermal condition (180 °C, 4 h). After that, the solution was given a filter treatment (0.1 μm, nylon), and then a reddish-brown CQDs suspension was obtained.

2.1.3. Preparation of CQDs/BOC Composites

A total of 0.25 g BOC was added to 70 mL deionized water with ultrasonic dispersant for 15 min. Subsequently, a certain volume of CQDs suspension was dropped into above mixture. Then, the mixtures were sealed in a Teflon-lined stainless-steel autoclave and heated at the temperature 180 °C under autogenous pressure for 4h. After natural cooling to room temperature, the product was filter centrifuged, washed with deionized water and ethyl alcohol and dried at 70 °C in an oven to obtain CQD/BOC composites. To study the impact of the CQDs content on the photocatalytic performance of the composites, a series of the CQD/BOC composites were obtained by adjusting the volumes of CQDs suspension (5, 10, 15 and 20 mL). The specimens were correspondingly labeled as BOC-CQD-5, BOC-CQD-10, BOC-CQD-15, BOC-CQD-20.

2.1.4. Fabrication of CQD/BOC Membranes

A total of 0.025 g BOC or CQD/BOC was added to 150 mL deionized water with ultrasonic dispersant for 15 min. The mixtures were filtered at 0.1 μm nylon membrane by vacuum pump. The BOC or CQD/BOC photocatalytic thin-film on the nylon membrane was obtained. The CQD/BOC membranes were fabricated, as illustrated in Figure 1.

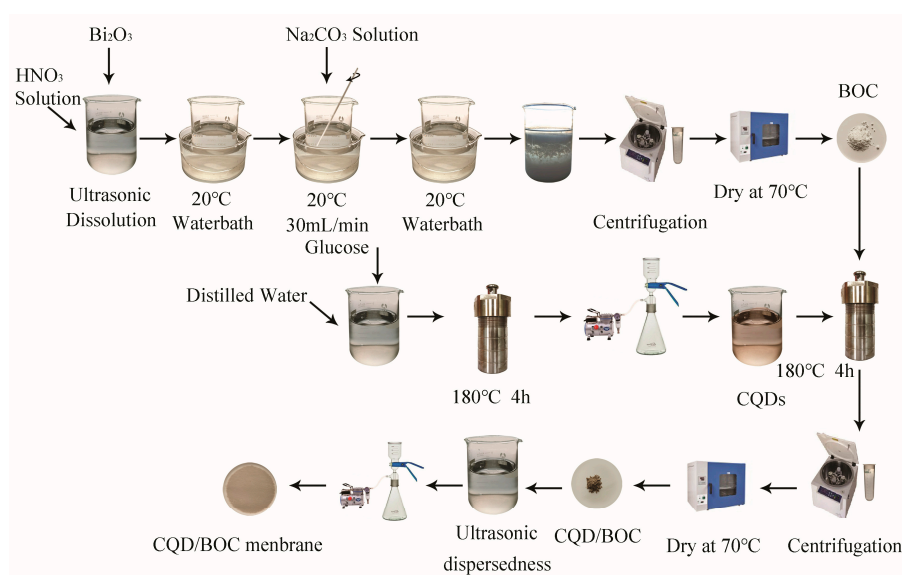


Figure 1. Chemical route for the preparation of carbon quantum dots (CQD)/ $\text{Bi}_2\text{O}_2\text{CO}_3$ (BOC) membrane.

2.2. Characterization

The powder X-ray diffraction (XRD) patterns were obtained from a diffractometer (D8-Advance, Bruker, Karlsruhe, Germany) using monochromatized $\text{Cu K}\alpha$ ($\lambda = 1.54056$ nm) radiation with scanning speed of $0.15^\circ/\text{s}$. The morphology of the samples was carried out on a scanning electron microscope (JSM-7001F, JEOL, Tokyo, Japan) operating at a 5 kV and a high-resolution transmission emission electron microscope (JEM-2100F, JEOL, Tokyo, Japan). The XPS spectra measurements were conducted on an X-ray photoelectron spectroscopy (ESCALAB 250Xi, Thermo Fisher, California, USA). The specific

surface area was measured on an automated gas sorption analyzer (AutosorbIQ2, Quantachrome, Florida, USA). UV-Vis diffuser reflectances (DRS) were carried out on a UV-Vis spectrometer (Lambda 950, PerkinElmer, Massachusetts, USA).

2.3. Photocatalytic test

The photocatalytic properties of the specimen were evaluated by toluene removal in air using a gas phase photocatalysis system (FPCS-1, Beijing Ferren Science & Technology Co., Ltd., Beijing, China). Before the photocatalytic test, the inter space of the reactor was first substituted with nitrogen to expel the oxygen and moisture. Toluene standard gas with concentration of 94.3 ppm in air was used as reactant. The BOC or CQD/BOC membrane was placed at the bottom of the reactor. Toluene standard gas was pumped into the chamber (about 450 mL). Then, the reactor was kept in dark for 30 min to reach the adsorption equilibrium. An incident light source (a 300W xenon lamp) was placed above the reactor which has a quartzose cover as an upper surface. At regular time intervals, the mixture gas in reactor was analyzed by gas chromatograph equipped with two flame-ionization detectors (FID). Toluene analysis was carried out with FID loaded with an Rt-Q-Bond Plot column (30 m × 0.25 mm, film thickness 10 μm), while CO₂ analysis was carried out with the other FID loaded with a packed column (TDX-01, 3 m × 3 mm), followed by a methanizer CO₂ concentration. The gas samples were fed to GC online through an automatic gas sampling valve. The temperature of the reactor was controlled using circulating cooling water to avoid thermal effect during the degradation process.

3. Results and Discussion

3.1. Morphology Analysis

The morphologies of the as-prepared BOC and CQD/BOC samples were observed by SEM and TEM. It is clear that the morphologies of the pure BOC were flower-like shape with a diameter of ca. 6 μm (Figure 2a), and the irregular flaky structures of BOC nanosheets gathered together with a diameter of ca. 500 nm (Figure S1a). The morphologies of CQD/BOC were flower-like shapes (Figure 2c–f), irregular flaky structures (Figure 2b and Figure S1b) and fine spherical particles (Figure 2d and Figure S1c). Thus, more reactive sites could be provided, due to the higher surface-to-volume ratio of BOC and CQD/BOC.

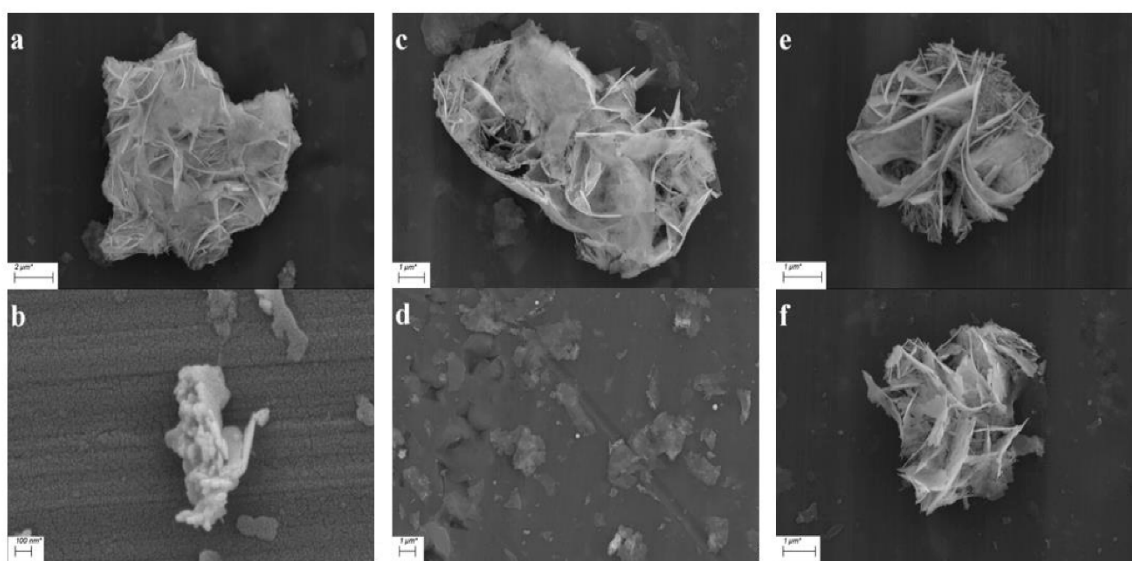


Figure 2. SEM images of BOC (a), BOC-CQD-5 (b), BOC-CQD-10 (c,d), BOC-CQD-15 (e) and BOC-CQD-20 (f).

The BET surface area test results of as-prepared samples are shown in Table 1. It was found that the specific surface area and pore volume of the sample by chemical route were much larger than the BOC by a hydrothermal method [35]. The specific surface area and pore volume of CQD/BOC were about 50% larger than BOC. They are similar to flower-like $\text{Bi}_2\text{O}_2\text{CO}_3$ [34]. Therefore, the larger BET surface area of CQD/BOC may result in better photocatalytic performance by providing more active sites than BOC sample.

Table 1. Specific surface area of BOC and CQD/BOC.

	BOC	BOC-CQD-5	BOC-CQD-10	BOC-CQD-15	BOC-CQD-20
Surface area (m^2/g)	12.293	17.189	18.842	17.699	17.266
Total pore volume for pores with Diameter less than 194.68 nm at $P/P_0 = 0.990027$ (cm^3/g)	0.0952	0.1441	0.1254	0.1248	0.0934

The morphology of BOC-CQD-15 was also observed by TEM and HRTEM (Figure 3 and Figure S2). As shown in Figure S2, the main morphology of sample was flower-like shape. Simultaneously, there are some fine spherical particles and irregular flaky structures, which is in accordance with SEM results. To further elucidate the element distribution of BOC-CQD-15, energy-dispersive X-ray elemental mappings were employed (Figure 3b–d), where Bi, O and C elements were uniformly distributed in the obtained sample. These mapping images correspond to the TEM image shown in Figure 3a. To determine the C element content, the EDS spectrums of the spectrum 4 and 5 in Figure 3g were measured. The C element content of spectrum 4 was 78.68%, which was much larger than 55.38% of spectrum 5. It revealed that the deep color dots were carbon quantum dots with the diameter of ca. 5–30 nm. Additionally, in Figure 3e,f, the (013) crystalline of BOC could be found in BOC-CQD-15 according to the lattice spacing of 0.291 nm (JCPDS 41-1488). Furthermore, a lattice spacing of 0.320 nm could also prove that the introduction of CQDs (004) according to JCPDS 26-1080. The result further indicates that CQDs were successfully modified on the surface of $\text{Bi}_2\text{O}_2\text{CO}_3$.

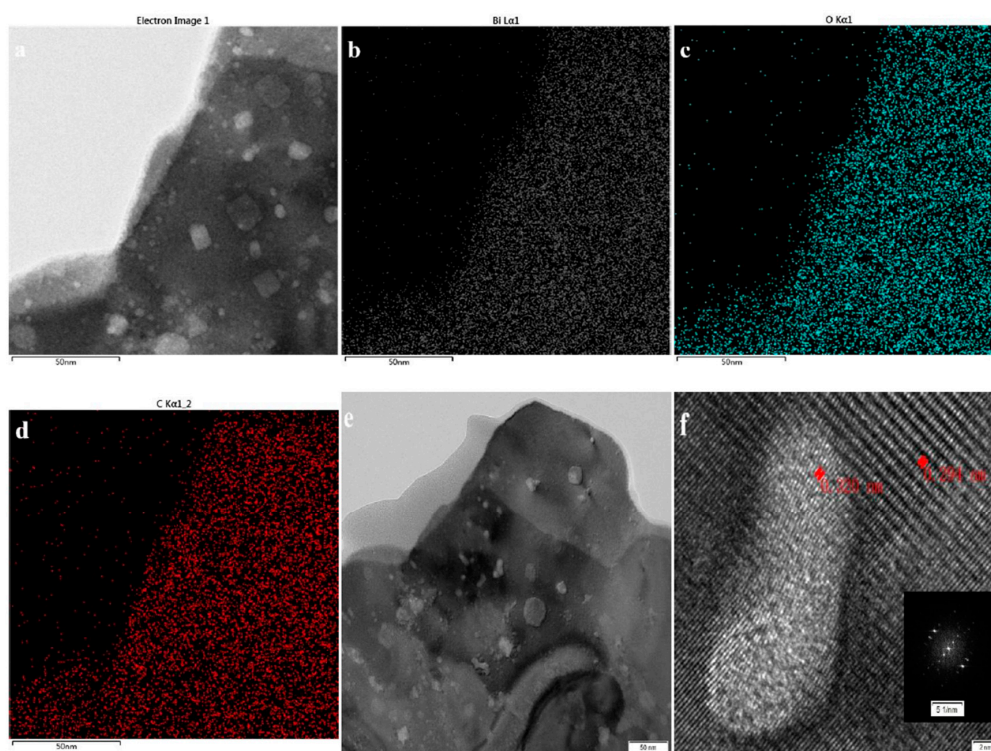


Figure 3. Cont.

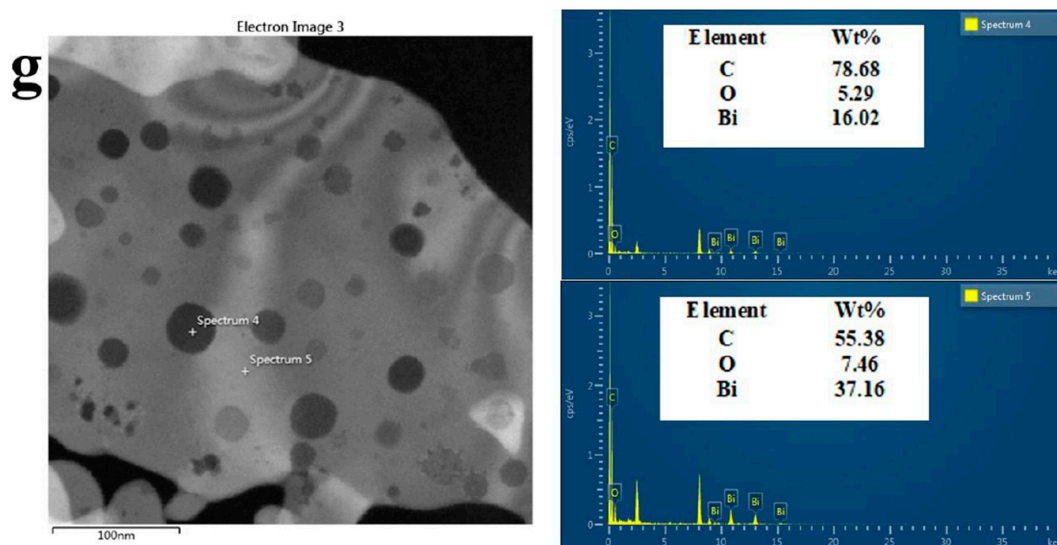


Figure 3. Element mapping images (a–d), HRTEM images (e,f) and EDS spectrum (g) of BOC-CQD-15.

3.2. Structure and Composition Analysis

The phase structure of the obtained BOC and CQD/BOC samples were detected by X-ray powder diffraction (XRD), and the results are shown in Figure 4. It reveals that all diffraction peaks of different samples could be well indexed to the pure phase of $\text{Bi}_2\text{O}_2\text{CO}_3$ (JCPDS 41-1488), without impurity peaks. The diffracted intensity ratio of (002)/(013) in the BOC, BOC-CQD-5, BOC-CQD-10, BOC-CQD-15 and BOC-CQD-20 were 59.50%, 65.17%, 52.74%, 76.95% and 83.55%, respectively, which were much larger than 25% of the primitive BOC standard card (JCPDS 41-1488). (002) facet was exposed dominantly, which might contribute to the separation of photo-excited hole-electron pairs [36].

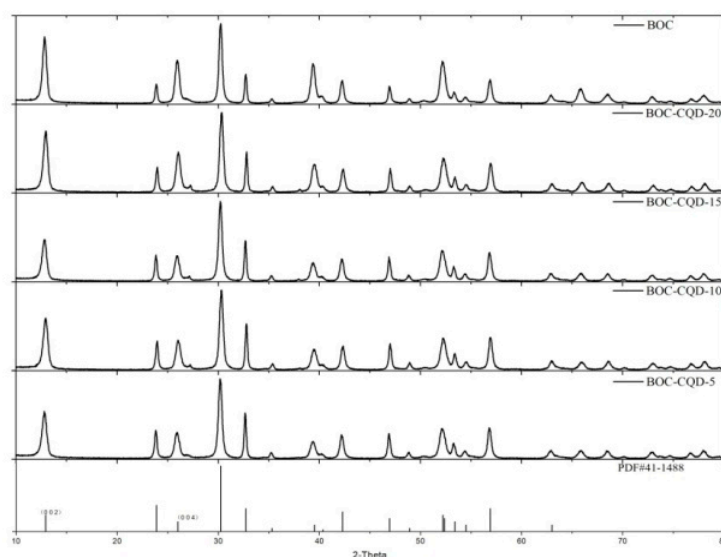


Figure 4. X-ray diffraction (XRD) patterns of as-prepared samples.

X-ray photoelectron spectroscopy (XPS) was conducted to investigate the chemical composition and surface electron state of the CQD/BOC samples (Figure 5 and Figure S3). Figure 5a demonstrated the typical survey spectrum of the as-obtained samples, showing that all of the samples consisted solely of Bi, O and C. The high-resolution XPS spectra of C1s, O1s and Bi4f for the obtained photocatalysts are shown in Figure 5b–f. In Figure 5b, the C1s peak at a binding energy of 284.8 eV can be attributed to the C–C bond with sp^2 orbital; the peak observed at 289.0 eV should be ascribed to the C–O bond in

$\text{Bi}_2\text{O}_2\text{CO}_3$ [37]. The spectra of O1s can be fitted into three Gaussian-Lorentzian peaks (see Figure 5c and Figure S1). The peak located at 529.8 eV is ascribed to the lattice oxygen in Bi–O binding energy, and the peaks at 530.7 eV and 531.6 eV can be assigned to carbonate and the surface hydroxyl groups on the surface of $\text{Bi}_2\text{O}_2\text{CO}_3$ [14,38]. In Figure 5d–f, the two apparent characteristic peaks for Bi-4f located at 159.1eV and 164.4 eV are attributed to $\text{Bi-4f}_{7/2}$ and $\text{Bi-4f}_{5/2}$ in $\text{Bi}_2\text{O}_2\text{CO}_3$, indicating the existence of Bi^{3+} in the samples. The $\text{Bi-4f}_{7/2}$ and $\text{Bi-4f}_{5/2}$ of CQD/BOC have a negative shift to low binding energy compared with BOC, indicating the higher electron density around Bi elements in CQD/BOC samples, and proving CQDs modified on the surface of $\text{Bi}_2\text{O}_2\text{CO}_3$ [39,40].

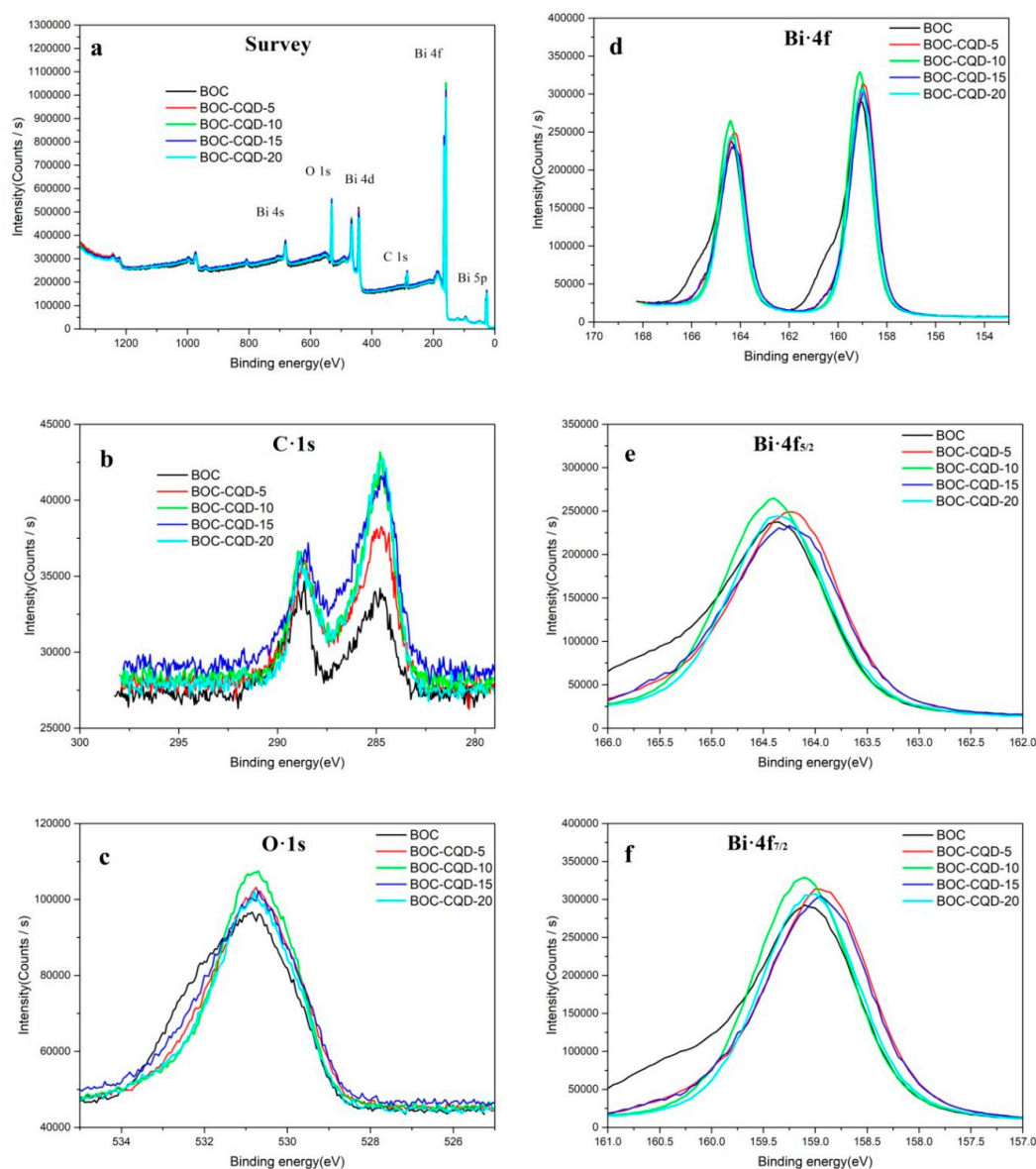


Figure 5. X-ray photoelectron spectroscopy (XPS) spectra of BOC samples: survey scan (a), C1s (b), O1s (c), and Bi-4f (d–f).

3.3. Photocatalytic Properties

The photocatalytic properties of the as-prepared samples were investigated through removing gaseous toluene (94.3 ppm) in air under the irradiation of an incident light source. As shown in Figure 6a, the pure BOC achieved a good photocatalytic performance with a removal rate of 70%, which can be attributed to (002) crystal face exposed. However, CQD/BOCs were superior to the pure

BOC, with a removal rate of up to 95%, which can be attributed to CQDs and (002) crystal face. The photocatalytic property of BOC-CQD-15 reached 96.62% after three hours irradiation.

In order to get a deeper understanding of the degradation reaction of toluene in air, the degradation products were detected using gas chromatograph (GC) with flame-ionization detectors (FID). The results are shown in Figure 6b and Figure S4. The CO₂ productivity of BOC-CQD-15 was 38.5 μmol, which is 2.4 times of the pure BOC and was the highest in all the CQD/BOCs.

On the basis of the toluene removal rate and the CO₂ productivity, the photocatalytic property of BOC-CQD-15 was the best in all the CQD/BOCs.

In order to observe the photo response range of CQD/BOC, the photocatalytic properties of BOC-CQD-15 were investigated through its ability of toluene decomposition under the irradiation of infrared light, visible light and ultraviolet light (showed in Figure 6c). BOC-CQD-15 has not response to IR light and Vis light, but it has response to UV light.

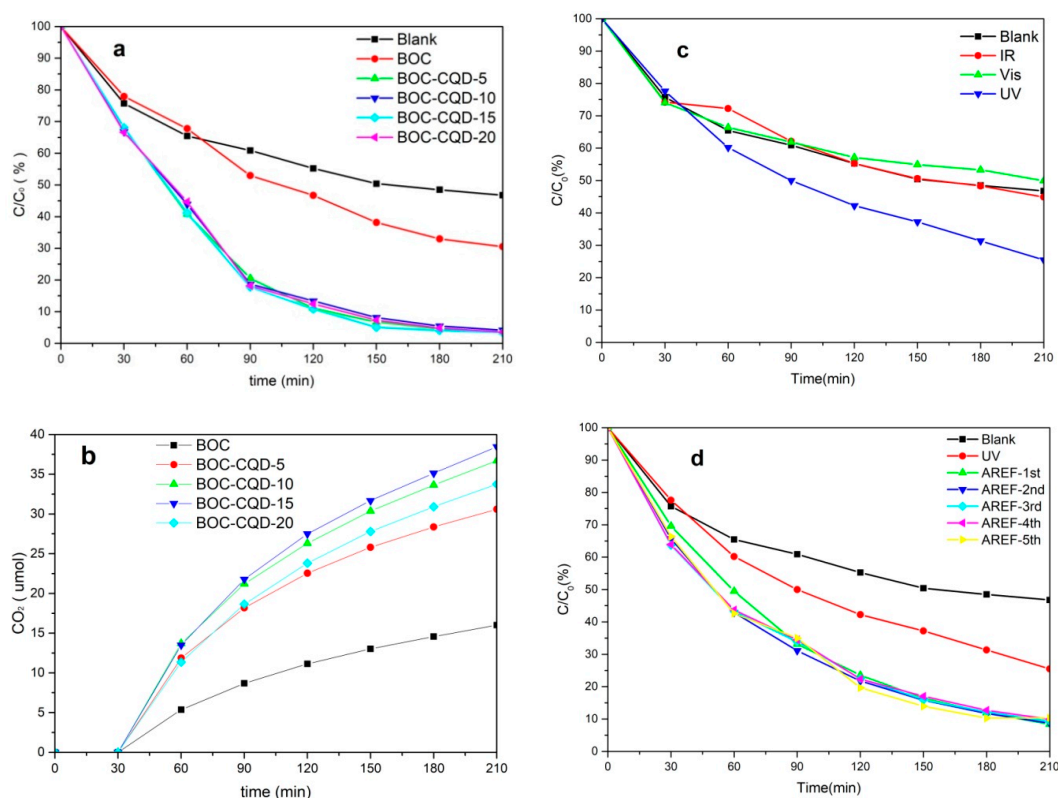


Figure 6. The photocatalytic properties of the as-prepared samples for toluene removal in air (a), the CO₂ productivity of the samples (b), the ability of BOC-CQD-15 under IR, Vis, UV irradiation (c) and the stability of BOC-CQD-15 under full light during five cycles (d).

The stability of photocatalytic degradation of toluene in air was observed by repeating the experiment for five runs under full spectrum after ultraviolet irradiation, and the result is shown in Figure 6d and Figure S5. It was clear that the photocatalytic property of BOC-CQD-15 under full spectrum was superior to its property under ultraviolet due to the outstanding up-converted photoluminescence peculiarity of carbon quantum dots modified on the surface of Bi₂O₂CO₃, which further extend the photoresponse range of BOC to the near infrared light. The BOC-CQD-15 could remain a constant photocatalytic performance as high as 90% in terms of removing toluene under incident light irradiation after five recycling runs. This phenomenon revealed a good recyclability of BOC-CQD-15 for toluene removal.

3.4. Photocatalytic Degradation Mechanism

The UV-Vis diffuse reflectance spectra of the samples were examined, and the results presented in Figure 7. It can be seen that the bandgap of all the samples can be decided about (3.4~3.5) eV. The results reveal that the CQD scarcely influence the light absorption of BOC or change the band gap of samples obviously.

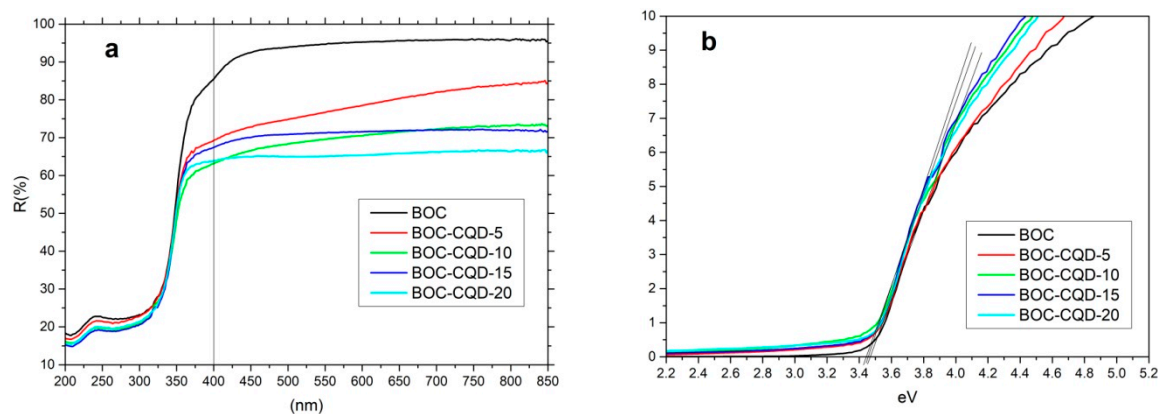


Figure 7. UV-Vis diffuse reflectance spectra of as-prepared samples (a) and band gap fitting with KMrelation (b).

According to the characterization of chromatogram, CO_2 is the primary product, and there is a little of CO during toluene degradation reaction. The CO productivity of BOC-CQD-15 was $6.33 \mu\text{mol}$, which was 2.5 times of the pure BOC (showed in Figure S4b). No other byproducts or intermediate were detected. It indicated that the main products of toluene degradation were CO_2 and H_2O and there was a modicum of CO.

The photocatalytic degradation mechanism of VOCs in air is slightly different from that in aqueous solution. A possible photocatalytic mechanism of the CQD/BOC composites toward the removal of toluene under simulated sunlight irradiation is schematically depicted in Figure 8. The BOC can effectively respond to the light with the wavelength shorter than about 400 nm. When the CQD/BOC photocatalyst reacts to the photons, the electrons are excited from the valence band to the conduction band of BOC, thus producing electron-hole pairs. Simultaneously, it is generally accepted that carbon quantum dots are an outstanding up-converted photoluminescence material. The up-converted emissions are usually located at shorter wavelengths in the range of 300–650 nm [38]. As a result, a part of the up-converted emissions of CQDs can in turn excite BOC to generate additional photo excited charges, further extending the photoresponse range of BOC to the NIR light. Meanwhile, CQDs can also be excited by absorbing visible light, the π electrons or σ electrons are excited to the lowest unoccupied molecular orbital (LUMO) [41,42]. The excited CQDs can act as excellent electron donors and acceptors. Consequently, the CB electrons in BOC would transfer to CQDs (π or σ orbital), which help with the separation and the migration of photo excited carriers.

The photogenerated electrons which migrate to the surface of BOC and CQDs reduce the surface-adsorbed O_2 to highly active species $\bullet\text{O}_2^-$. Thus, highly active $\bullet\text{O}_2^-$ oxidizes toluene to CO_2 , H_2O and other intermediate products, such as benzene, benzoic acid, benzaldehyde and benzyl alcohol [43]. Then h^+ on the surface of BOC oxidizes the surface-adsorbed H_2O to highly active species $\bullet\text{OH}$, and the active species ($\bullet\text{O}_2^-$ and $\bullet\text{OH}$) oxidizes the adsorbed intermediates to CO_2 and H_2O , consequently forming the final products CO_2 and H_2O .

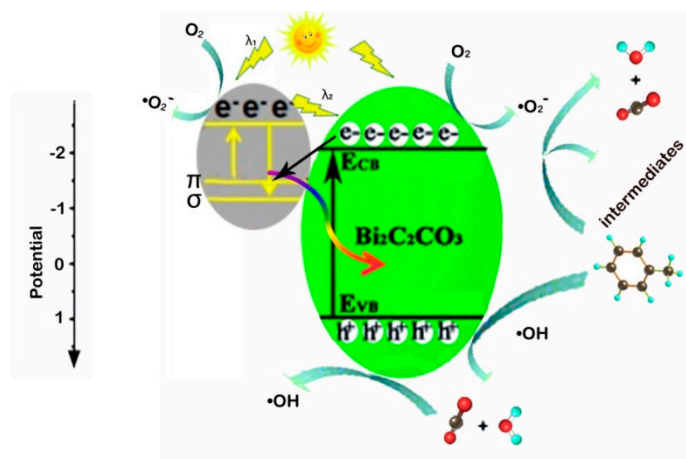


Figure 8. Photocatalytic mechanism of toluene removal for BOC-CQD-15.

4. Conclusions

In summary, (002) oriented flower-like $\text{Bi}_2\text{O}_2\text{CO}_3$ composites were synthesized by a facile chemical route and carbon quantum dots were modified on their surface through a hydrothermal method. The synthesized composites (CQD/BOC) have three morphologies, which were flower-like shapes, irregular flaky structures and fine spherical particles. Through HRTEM characterization, it was proved that CQDs were modified successfully on the surface of $\text{Bi}_2\text{O}_2\text{CO}_3$. Photocatalytic mineralization of toluene in air over CQD/BOC was measured. The effect of BOC-CQD-15 was optimum, and as a result, the toluene removal rate was up to 96.62% in three hours under full light irradiation, the rate was still up to 90% after five recycling runs in terms of stability. CO_2 was verified to be the main product after reaction. Better performance can be contributed to (0 0 2) facet orientation evolution and CQDs modified on the surface of $\text{Bi}_2\text{O}_2\text{CO}_3$, which enhance the efficient separation of photogenerated electron-holes.

Supplementary Materials: The following are available online at <http://www.mdpi.com/2079-4991/10/9/1795/s1>, Figure S1: SEM images of BOC (a) and BOC-CQD-10 (b,c); Figure S2: TEM images of BOC-CQD-15 (a–d); Figure S3: XPS spectra of BOC samples: O1s; Figure S4: The CO_2 productivity (a), the CO productivity (b), the total productivity of $\text{CO}_2 + \text{CO}$ (c), the rate of CO_2/CO (d) of the as-prepared samples for toluene removal in air; Figure S5: The photo images of BOC-CQD-15 under IR, Vis, UV, and full light irradiation during five cycles: before (a) and after (b).

Author Contributions: Investigation, J.D., H.W., Y.X. and Y.L. (Yidong Luo); Methodology, J.D., H.W. and Y.G.; Supervision, H.W. and Y.L. (Yuanhua Lin); Writing and original draft, J.D. and J.L.; Review & editing, Y.L. (Yidong Luo) and R.L. All authors have read and agreed to the published version of the manuscript.

Funding: This work was supported by the National Natural Science Foundation of China (Grant No. 51532002 and 51532003).

Conflicts of Interest: The authors declare no conflict of interest.

References

1. Brown, S.; Sim, M.R.; Abramson, M.J.; Gray, C.N. Concentrations of volatile organic compounds in indoor air—A review. *Indoor Air* **1994**, *4*, 123–134. [[CrossRef](#)]
2. Jones, A.P. Indoor air quality and health. *Atmos. Environ.* **1999**, *33*, 4535–4564. [[CrossRef](#)]
3. Wolkoff, P. Trends in Europe to reduce the indoor air pollution of VOCs. *Indoor Air* **2003**, *13*, 5–11. [[CrossRef](#)] [[PubMed](#)]
4. Haghghat, F.; Lee, C.-S.; Pant, B.; Bolourani, G.; Lakdawala, N.; Bastani, A. Evaluation of various activated carbons for air cleaning—Towards design of immune and sustainable buildings. *Atmos. Environ.* **2008**, *42*, 8176–8184. [[CrossRef](#)]
5. Siegel, J. Primary and secondary consequences of indoor air cleaners. *Indoor Air* **2016**, *26*, 88–96. [[CrossRef](#)]
6. Huang, H.; Xu, Y.; Feng, Q.; Leung, D.Y. Low temperature catalytic oxidation of volatile organic compounds: A review. *Catal. Sci. Technol.* **2015**, *5*, 2649–2669. [[CrossRef](#)]

7. Huang, Y.; Ho, S.; Lu, Y.; Niu, R.; Xu, L.; Cao, J.; Lee, S. Removal of indoor volatile organic compounds via photocatalytic oxidation: A short review and prospect. *Molecules* **2016**, *21*, 56. [[CrossRef](#)]
8. Hamza, M.A.; El-Shazly, A.N.; Tolba, S.A.; Allam, N.K. Novel Bi-based photocatalysts with unprecedented visible light-driven hydrogen production rate: Experimental and DFT insights. *Chem. Eng. J.* **2019**, *384*, 123351. [[CrossRef](#)]
9. Li, M.; Huang, H.; Yu, S.; Tian, N.; Zhang, Y. Facet, junction and electric field engineering of bismuth-based materials for photocatalysis. *ChemCatChem* **2018**, *10*, 4477–4496. [[CrossRef](#)]
10. Zhang, L.; Yang, J.; Zhao, X.; Xiao, X.; Sun, F.; Zuo, X.; Nan, J. Small-molecule surface modified bismuth-based semiconductors as a new class of visible-light-driven photocatalytic materials: Structure-dependent photocatalytic properties and photosensitization mechanism. *Chem. Eng. J.* **2020**, *380*, 122546. [[CrossRef](#)]
11. Li, L.; Yang, Y.; Li, G.; Zhang, L. Conversion of a Bi nanowire array to an array of Bi-Bi₂O₃ core-shell nanowires and Bi₂O₃ nanotubes. *Small* **2006**, *2*, 548–553. [[CrossRef](#)] [[PubMed](#)]
12. Sun, R.; Shi, Q.; Zhang, M.; Xie, L.; Chen, J.; Yang, X.; Chen, M.; Zhao, W. Enhanced photocatalytic oxidation of toluene with a coral-like direct Z-scheme BiVO₄/g-C₃N₄ photocatalyst. *J. Alloy. Compd.* **2017**, *714*, 619–626. [[CrossRef](#)]
13. Wang, Y.; Jianga, S.; Liu, F.; Zhao, C.; Zhao, D.; Li, X. Study on preparation and toluene removal of BiOI/Bi₂WO₆/ACF photocatalyst. *Appl. Surf. Sci.* **2019**, *488*, 161–169. [[CrossRef](#)]
14. Fan, W.; Li, H.; Zhao, F.; Xiao, X.; Huang, Y.; Ji, H.; Tong, Y. Boosting photocatalytic performance of (001) BiOI: Enhance donor density and separation efficiency of the photogenerated electrons and holes. *Chem. Commun.* **2016**, *52*, 5316–5319. [[CrossRef](#)] [[PubMed](#)]
15. Liu, H.; Chen, P.; Yuan, X.; Zhang, Y.; Huang, H.; Wang, L.; Dong, F. Pivotal roles of artificial oxygen vacancies in enhancing photocatalytic activity and selectivity on Bi₂O₂CO₃ nanosheets. *Chin. J. Catal.* **2019**, *40*, 620–630. [[CrossRef](#)]
16. Chen, L.; Huang, R.; Yin, S.-F.; Luo, S.-L.; Au, C.-T. Flower-like Bi₂O₂CO₃: Facile synthesis and their photocatalytic application in treatment of dye-containing wastewater. *Chem. Eng. J.* **2012**, *123*, 193–194. [[CrossRef](#)]
17. Cheng, H.; Huang, B.; Yang, K.; Wang, Z.; Qin, X.; Zhang, X.; Dai, Y. Facile template-free synthesis of Bi₂O₂CO₃ hierarchical microflowers and their associated photocatalytic activity. *Chemphyschem* **2010**, *11*, 2167–2173. [[CrossRef](#)]
18. Wang, F.; Zhao, Z.; Zhang, K.; Dong, F.; Zhou, Y. Topochemical transformation of low energy crystal facets to high energy facets: A case from Bi₂O₂CO₃ {001} facets to β-Bi₂O₃ {001} facets with improved photocatalytic oxidation of NO. *Cryst. Eng. Comm.* **2015**, *17*, 6098–6102. [[CrossRef](#)]
19. Hao, W.; Teng, F.; Gu, W.; Liu, Z.; Zhang, A.; Liu, Z. Investigation on the effect of an anion layer on photocatalytic activity: Carbonate vs. oxalate. *New J. Chem.* **2017**, *41*, 7073–7080. [[CrossRef](#)]
20. Madhusudan, P.; Ran, J.; Zhang, J.; Yu, J.; Liu, G. Novel urea assisted hydrothermal synthesis of hierarchical BiVO₄/Bi₂O₂CO₃ nanocomposites with enhanced visible-light photocatalytic activity. *Appl. Catal. B Environ.* **2011**, *110*, 286–295. [[CrossRef](#)]
21. Zhao, T.Y.; Zai, J.T.; Miao, X.; Zou, Q.; Su, Y.Z.; Wang, K.X.; Qian, X.F. Hierarchical Bi₂O₂CO₃ Microspheres with Improved Visible-Light-Driven Photocatalytic Activity. *Cryst. Eng. Comm.* **2011**, *13*, 4010–4017. [[CrossRef](#)]
22. Zhang, G.; Wang, J.; Shen, X.; Wang, J.; Wang, B.; Gao, D. Br-doped Bi₂O₂CO₃ nanosheets with improved electronic structure and accelerated charge migration for outstanding photocatalytic behavior. *Appl. Surf. Sci.* **2019**, *470*, 63–73. [[CrossRef](#)]
23. Li, J.; Liu, Y.; Zhou, Y.; Liu, S.; Liang, Y.; Luo, T.; Dai, G. Enhanced visible-light photocatalytic activity of Bi₂O₂CO₃ nanoplates by Fe-doping in the degradation of rhodamine B. *Mater. Res. Bull.* **2018**, *107*, 438–445. [[CrossRef](#)]
24. Lan, Y.; Li, Z.; Xie, W.; Li, D.; Yan, G.; Guo, S.; Pan, C.; Wu, J. In situ fabrication of I-doped Bi₂O₂CO₃/g-C₃N₄ heterojunctions for enhanced photodegradation activity under visible light. *J. Hazard. Mater.* **2020**, *385*, 121622. [[CrossRef](#)]
25. Huang, H.; Wang, J.; Dong, F.; Guo, Y.; Tian, N.; Zhang, Y.; Zhang, T. Highly Efficient Bi₂O₂CO₃ Single-Crystal Lamellas with Dominantly Exposed {001} Facets. *Cryst. Growth Des.* **2015**, *15*, 534–537. [[CrossRef](#)]

26. Zhao, Z.; Zhou, Y.; Wang, F.; Zhang, K.; Yu, S.; Cao, K. Polyaniline-decorated {001} facets of $\text{Bi}_2\text{O}_2\text{CO}_3$ nanosheets: In situ oxygen vacancy formation and enhanced visible light photocatalytic activity. *ACS Appl. Mater. Interfaces* **2015**, *7*, 730–737. [[CrossRef](#)]
27. Yang, C.; Xue, Z.; Qin, J.; Sawangphruk, M.; Rajendran, S.; Zhang, X.; Liu, R. Visible Light-Driven Photocatalytic H₂ Generation and Mechanism Insights into $\text{Bi}_2\text{O}_2\text{CO}_3/\text{g-C}_3\text{N}_4$ Z-Scheme Photocatalyst. *J. Phys. Chem. C* **2019**, *123*, 4795–4804. [[CrossRef](#)]
28. Fan, H.; Zhou, H.; Li, H.; Liu, X.; Ren, C.; Wang, F.; Li, W. Novel $\text{Ag}_2\text{CrO}_4/\text{Bi}_2\text{O}_2\text{CO}_3$ heterojunction: Simple preparation, wide visible light absorption band and excellent photocatalytic activity. *Chem. Phys.* **2019**, *517*, 60–66. [[CrossRef](#)]
29. Duan, Y.; Li, J.; Li, Y.; Shang, X.; Jia, D.; Li, C. Direct Z-scheme $\text{Bi}_2\text{O}_2\text{CO}_3$ /porous g- C_3N_4 heterojunction for improved photocatalytic degradation performance. *J. Taiwan Inst. Chem. Eng.* **2020**, *106*, 74–85. [[CrossRef](#)]
30. Tian, J.; Leng, Y.; Zhao, Z.; Xia, Y.; Sang, Y.; Hao, P.; Zhan, J.; Li, M.; Liu, H. Carbon quantum dots/hydrogenated TiO_2 nanobelt heterostructures and their broad spectrum photocatalytic properties under UV, visible, and near-infrared irradiation. *Nano Energy* **2015**, *11*, 419–427. [[CrossRef](#)]
31. Li, H.; Liu, R.; Liu, Y.; Huang, H.; Yu, H.; Ming, H.; Lian, S.; Lee, S.-T.; Kang, Z. Carbon quantum dots/ Cu_2O composites with protruding nanostructures and their highly efficient (near) infrared photocatalytic behavior. *J. Mater. Chem.* **2012**, *22*, 17470–17475. [[CrossRef](#)]
32. Zhang, H.; Ming, H.; Lian, S.; Huang, H.; Li, H.; Zhang, L.; Liu, Y.; Kang, Z.; Lee, S.-T. Fe_2O_3 /carbon quantum dots complex photocatalysts and their enhanced photocatalytic activity under visible light. *Dalton Trans.* **2011**, *40*, 10822–10825. [[CrossRef](#)] [[PubMed](#)]
33. Zhang, H.; Huang, H.; Ming, H.; Li, H.; Zhang, L.; Liu, Y.; Kang, Z. Carbon quantum dots/ Ag_3PO_4 complex photocatalysts with enhanced photocatalytic activity and stability under visible light. *J. Mater. Chem.* **2012**, *22*, 10501–10506. [[CrossRef](#)]
34. Bai, P.; Tong, X.; Wan, J.; Gao, Y.; Xue, S. Flower-like $\text{Bi}_2\text{O}_2\text{CO}_3$ -mediated selective oxidative coupling processes of amines under visible light irradiation. *J. Catal.* **2019**, *374*, 257–265. [[CrossRef](#)]
35. Ding, J.; Wang, H.; Xu, H.; Qiao, L.; Luo, Y.; Lin, Y.; Nan, C. Synthesis and broadband spectra photocatalytic properties of $\text{Bi}_2\text{O}_2(\text{CO}_3)_{1-x}\text{S}_x$. *Materials* **2018**, *11*, 791. [[CrossRef](#)] [[PubMed](#)]
36. Ding, J.; Wang, H.; Luo, Y.; Xu, Y.; Liu, J.; Lin, Y. (002) Oriented $\text{Bi}_2\text{O}_2\text{CO}_3$ nanosheets with enhanced photocatalytic performance for toluene removal in air. *Catalysts* **2020**, *10*, 389. [[CrossRef](#)]
37. Xian, T.; Sun, X.; Di, L.; Zhou, Y.; Ma, J.; Li, H.; Yang, H. Carbon Quantum Dots (CQDs) decorated $\text{Bi}_2\text{O}_{3-x}$ hybrid photocatalysts with promising nir-light-driven photodegradation activity for AO7. *Catalysts* **2019**, *9*, 1031. [[CrossRef](#)]
38. Liang, N.; Wang, M.; Jin, L.; Huang, S.; Chen, W.; Xu, M.; He, Q.; Zai, J.; Fang, N.; Qian, X. Highly efficient $\text{Ag}_2\text{O}/\text{Bi}_2\text{O}_2\text{CO}_3$ p-n heterojunction photocatalysts with improved visible-light responsive activity. *ACS Appl. Mater. Interfaces* **2014**, *6*, 11698–11705. [[CrossRef](#)]
39. Wang, C.; Shao, C.; Liu, Y.; Zhang, L. Photocatalytic properties BiOCl and Bi_2O_3 nanofibers prepared by electrospinning. *Scr. Mater.* **2008**, *59*, 332–335. [[CrossRef](#)]
40. Houc, W.; Hu, T.; Du, N.; Zhang, R.; Liu, J.-Q.; Hou, W. Wavelength-dependent differences in photocatalytic performance between BiOBr nanosheets with dominant exposed (001) and (010) facets. *Appl. Catal. B Environ.* **2016**, *187*, 342–349.
41. Li, H.T.; Kang, Z.H.; Liu, Y.; Lee, S.T. Carbon nanodots: Synthesis, properties and applications. *J. Mater. Chem.* **2012**, *22*, 24230–24253. [[CrossRef](#)]
42. Wang, S.Y.; Yang, H.; Yi, Z.; Wang, X.X. Enhanced photocatalytic performance by hybridization of Bi_2WO_6 nanoparticles with honeycomb-like porous carbon skeleton. *J. Environ. Manag.* **2019**, *248*, 109341. [[CrossRef](#)] [[PubMed](#)]
43. Hennezel, O.; Pichat, P.; Ollis, D.F. Benzene and toluene gas-phase photocatalytic degradation over H_2O and HCL pretreated TiO_2 : By-products and mechanisms. *J. Photochem. Photobiol. A Chem.* **1998**, *118*, 197–204. [[CrossRef](#)]

